Engineering craniofacial scaffolds

SJ Hollister
CY Lin
E Saito
CY Lin
RD Schek
JM Taboas
JM Williams
B Partee
CL Flanagan
A Diggs
EN Wilke
GH Van Lenthe
R Müller
T Wirtz
S Das
SE Feinberg
PH Krebsbach

Authors' affiliations:
S.J. Hollister, C.Y. Lin, E. Saito, C.Y. Lin, R.D. Schek, J.M. Williams, C.L. Flanagan, A. Diggs, E.N. Wilke, Skeletal Engineering Group, The University of Michigan, Ann Arbor, MI, USA
S.J. Hollister, C.Y. Lin, E. Saito, R.D. Schek, J.M. Williams, C.L. Flanagan, A. Diggs, E.N. Wilke, Department of Biomedical Engineering, The University of Michigan, Ann Arbor, MI, USA
S.J. Hollister, Department of Surgery, The University of Michigan, Ann Arbor, MI, USA
S.J. Hollister, C.Y. Lin, B. Partee, S. Das, Department of Mechanical Engineering, The University of Michigan, Ann Arbor, MI, USA
J.M. Taboas, Cartilage Biology and Orthopaedics Branch, National Institute of Musculoskeletal and Skin Diseases, Bethesda, MD, USA
G.H. Van Lenthe, R. Müller, Institute of Biomedical Engineering, ETH, Zurich, Switzerland
T. Wirtz, Fraunhofer Institute of Laser Technology, Aachen, Germany
S.E. Feinberg, Department of Oral and Maxillofacial Surgery, The University of Michigan, Ann Arbor, MI, USA
P.H. Krebsbach, Department of Oral Medicine, Pathology and Oncology, The University of Michigan, Ann Arbor, MI, USA

Structured Abstract:

Authors – Hollister SJ, Lin CY, Saito E, Lin CY, Schek RD, Taboas JM, Williams JM, Partee B, Flanagan CL, Diggs A, Wilke EN, Van Lenthe GH, Müller R, Wirtz T, Das S, Feinberg SE, Krebsbach PH

Objective – To develop an integrated approach for engineering craniofacial scaffolds and to demonstrate that these engineered scaffolds would have mechanical properties in the range of craniofacial tissue and support bone regeneration for craniofacial reconstruction.

Experimental Variable – Scaffold architecture designed to achieve desired elasticity and permeability. Scaffold external shape designed to match craniofacial anatomy.

Outcome Measure – Final fabricated biomaterial scaffolds. Compressive mechanical modulus and strength. Bone regeneration as measured by micro-CT scanning, mechanical testing and histology.

Setting – Departments of Biomedical Engineering, Oral/Maxillofacial Surgery, and Oral Medicine, Pathology and Oncology at the University of Michigan.

Results – Results showed that the design/fabrication approach could create scaffolds with designed porous architecture to match craniofacial anatomy. These scaffolds could be fabricated from a wide range of biomaterials, including titanium,

Correspondence to:
Scott J. Hollister, PhD
Departments of Biomedical Engineering, Surgery, and Mechanical Engineering
The University of Michigan
1107 Gerstacker Bldg., 2200 Bonisteel Blvd.
Ann Arbor, MI 48109, USA
Tel.: +1 734 647 9962
Fax: +1 734 936 1905
E-mail: scottho@umich.edu

Dates:
Accepted 10 April 2005

To cite this article:
Orthod Craniofacial Res **8**, 2005; 162–173
Hollister SJ, Lin CY, Saito E, Lin CY, Schek RD, Taboas JM, Williams JM, Partee B, Flanagan CL, Diggs A, Wilke EN, Van Lenthe GH, Müller R, Wirtz T, Das S, Feinberg SE, Krebsbach PH: Engineering craniofacial scaffolds

degradable polymers, and degradable calcium phosphate ceramics. Mechanical tests showed that fabricated scaffolds had compressive modulus ranging 50 to 2900 MPa and compressive strength ranging from 2 to over 56 MPa, within the range of human craniofacial trabecular bone. *In vivo* testing of designed scaffolds showed that they could support bone regeneration via delivery of BMP-7 transduced human gingival fibroblasts in a mouse model. Designed hydroxyapatite scaffolds with pore diameters ranging from 400 to 1200 microns were implanted in minipig mandibular defects for 6 and 18 weeks. Results showed substantial bone ingrowth (between 40 and 50% at 6 weeks, between 70 and 80% at 18 weeks) for all scaffolds, with no significant difference based on pore diameter.

Conclusion – Integrated image-based design and solid free-form fabrication can create scaffolds that attain desired elasticity and permeability while fitting any 3D craniofacial defect. The scaffolds could be manufactured from degradable polymers, calcium phosphate ceramics and titanium. The designed scaffolds supported significant bone regeneration for all pore sizes ranging from 300 to 1200 microns. These results suggest that designed scaffolds are clinically applicable for complex craniofacial reconstruction.

Key words: craniofacial; fabrication; image-based design; solid free-form; temporomandibular joint; tissue engineering

Introduction

Tissue engineering approaches to craniofacial skeletal reconstruction evoke the general principles of using porous scaffolds that deliver biofactors (cells, genes and proteins) to regenerate natural tissue. Craniofacial scaffolds must also fulfill the typical requirements for mechanically functioning tissues of enhancing tissue regeneration through biofactor delivery while maintaining temporary mechanical function until the tissue can bear load (1, 2). However, craniofacial scaffolds must fit very complex three-dimensional (3D) anatomic defects that can be much more complicated than those in the appendicular skeleton. Thus, the three basic requirements for craniofacial skeletal scaffolds are:

1. Fit complex 3D anatomic defects.
2. Provide temporary load bearing until tissue forms.
3. Enhance tissue regeneration through biofactor delivery.

Requirements 2 and 3 are coupled, leading to additional obstacles for scaffold engineering. A scaffold which can optimally deliver biofactors is extremely porous, while a scaffold that can provide temporary load bearing has typically small or no porosity. Craniofacial scaffolds must therefore fit complex anatomic defects, be porous enough to effectively deliver biofactors, and be dense enough for a long enough period to bear mechanical forces until the regenerate tissue can carry forces.

An engineering process that can fulfill the three requirements must be able to provide rigorous control over both scaffold exterior shape and interior porous architecture. This process should include design techniques that can utilize patient image data to create exterior shape and at the same time optimize porous scaffold architecture to provide the right balance between load bearing and biofactor delivery. This process should also include the capability to fabricate the undoubtedly complex 3D structures that will result from the design process.

Each of the three craniofacial scaffold requirements alone is complex. Furthermore, although definition of exterior shape may be gleaned by combination of

image data and surgical experience, the load bearing and regeneration requirements are more difficult to define. For example, the desired target for load bearing capability has not been experimentally determined, and it is likely to differ between anatomic sites. One measure of load bearing capability is the mechanical properties of native craniofacial tissue. It has been suggested that scaffold mechanical properties should be equivalent to those of native tissue (2) or should match at least some minimum value of native tissue (3). However, even with this measure there is little or no experimental data to suggest what percentage of native tissue mechanical properties that scaffold should possess, even if the focus is primarily on craniofacial bone and cartilage tissue.

For craniofacial bone, a wide range of elastic properties have been obtained, depending on species, age, anatomic location, and dentition. Anisotropic elastic moduli range for human mandibular cortical bone range from 11 000 to 30 000 MPa for mandibles with and without dentition (4–6). Anisotropic elastic moduli for human mandibular trabecular bone have been found to range from 120 to 450 MPa for the mandibular condyle (7, 8) and from 114 to 910 MPa for the mandible from the mid-line to the ramus (9). Macaque monkey mandibular cortical bone has anisotropic elastic moduli ranging from 9000 to 24 000 MPa (10), while mandibular cortical bone of canines was found to average 7500 MPa and be isotropic (11).

Obviously, craniofacial soft tissues are much more compliant than bone, but exhibit the same variability. One of the most widely studied craniofacial cartilage tissues is the temporomandibular joint (TMJ) disk. A recent review by Detamore and Athanasiou (12) found widely varying ranges for TMJ disk compressive modulus, with human TMJ disks having compressive moduli ranging from 1.8 to 60 MPa. Relative to TMJ disk cartilage, much less is known about the mechanical properties of mandibular condyle fibrocartilage. From Mao's group at the University of Illinois-Chicago, Hu et al. (13) found mature rabbit mandibular condyle fibrocartilage to have elastic moduli ranging from 0.9 to 2.5 MPa depending on anatomic location within the mandibular condyle, while Patel and Mao (14) found a narrow range of 0.9–1.2 MPa for 7-day-old rabbits. Thus, craniofacial cartilaginous tissues have exhibited elastic moduli ranging from 0.9 to 60.0 MPa. These elastic measurements, although complex in and of themselves, greatly simplify the true poroelastic behavior of cartilaginous tissues. Thus, depending on the definition of load carrying capability, scaffolds may need to exhibit elastic moduli ranging from 100 to 30 000 MPa for bone, and from 0.9 to 60 MPa for craniofacial cartilage tissues, a range of two orders of magnitude for bone and three orders of magnitude for cartilage.

A number of approaches for engineering craniofacial tissues have been reported that combine scaffolds with biofactors (see e.g. 15–17). These approaches have used hydrogel scaffolds or polymer scaffolds that have been made using traditional polymer processing techniques like porogen leaching or gas foaming. In general, these techniques have been able to successfully generate tissue in non-load bearing applications (18). However, the regenerate tissue has rarely been evaluated with regards to its mechanical performance nor have scaffolds with appropriate mechanical properties in the range of craniofacial tissues been used for craniofacial tissue engineering.

The purpose of this paper is to present an approach for engineering craniofacial and TMJ scaffolds that can fulfill the three basic requirements for successful *in vivo* tissue reconstruction. As such, it reviews an approach developed by our research groups over the last 4 years designing, fabricating and testing scaffolds for craniofacial reconstruction. This approach includes an image-based computational design method that can design any complex 3D anatomic shape as well as incorporating optimization approaches that achieve a balance between biofactor delivery and load bearing. This approach also includes a fabrication method that can create these scaffolds from the entire range of currently used biomaterials including metals, ceramics, polymers and composites thereof. Finally, we present initial *in vitro* and *in vivo* test data demonstrating that these designed scaffolds can provide adequate mechanical properties and also support bone and cartilage regeneration needed to reconstruct craniofacial structures.

Scaffold design

An approach for craniofacial scaffold design must include the capability to design scaffolds that fit anatomic defects defined from clinical imaging data

and the capability to design porous scaffold architecture that can balance load bearing and biofactor delivery requirements. To address these issues, we have developed an image-based design approach for designing tissue engineering scaffolds (1, 19). In image-based design, a master global image database is used to define the anatomic shape. This global image database, is then used as a template in which to position the porous architecture design. A second set of image database, termed local image database, are then used to define the porous scaffold architecture design. One local image database is created for each separate porous microstructure design, enabling the creation of scaffolds with heterogeneous structure. Although we typically use only two hierarchical database structures, local and global, this technique can readily be extended to handle any number of structural hierarchies, ranging from the nanometer scale to the tens of centimeter scale. The limitation is computational memory to handle the voxel data sets and the resolution of current fabrication systems, which currently extend only to the 100-micron range.

The global image design database can be created directly from a CT or MR image of a patient. The image resolution is first interpolated down to the desired local image design database resolution. The user can then selects the tissue defect region to be reconstructed and assigns this region a specific density value between 1 and 255. This density value will then serve as a flag indicating the 3D volume to be reconstructed. This reconstruction region selection may be carried out in standard image processing software like ANALYZE™ (Analyze Direct, Inc., Lenexa, KS, USA) or Interactive Data Language™ (IDL; Research Systems, Inc., Boulder, CO, USA). The base reconstruction region is now represented by a single density value within a voxel data set. This density value within and immediately adjacent to the base reconstruction region can then be modified to add adjunct surgical fixation regions and a heterogeneous region for mapping the designed microstructure.

Once the global image design database is created, the next question is how to design the porous microstructure. The specific requirements that pertain to scaffold microstructure design are the need for temporary load bearing (requirement 2) and the need to enhance tissue regeneration through biofactor delivery (requirement 3). Requirements 2 and 3 would dictate the scaffold architecture be as dense as possible for load bearing and as porous as possible for biofactor delivery, an obvious conflict. Therefore, we must be able to create an architecture design that balances the need for load bearing and biofactor delivery. Achieving balance means that we must be able to least compute a priori how scaffold architecture will affect load bearing and biofactor delivery, and preferably, achieve the optimal compromise between these two requirements. However, 'load bearing' and 'biofactor delivery' are qualitative terms for which we need specific quantitative measures if we are to perform computational design. Therefore, we have proposed the use of stiffness (more precisely, elastic modulus) as a measure of load bearing, and porosity and permeability as a measure of the capability to deliver biofactors. Although porosity is an indicator of how much space is available for seeding biofactors, it provides no indication whether the scaffold pores are *connected*, which is critical for increasing cell nutrition and allowing connected tissue growth.

Associating elastic modulus with load bearing and porosity/permeability with biofactor delivery is only a first step in quantitatively designing scaffolds that adequately balance load bearing and biofactor delivery. The next important step is the capability to compute effective scaffold modulus, porosity and permeability based on a proposed microstructure design. To make design more tractable, we will design locally periodic scaffold architectures based on a single unit cell (not to be confused with a biological cell, but rather a 3D mathematical entity). Local scaffold porosity may be easily calculated from a unit cell image design by simply dividing the number of voxels with solid material by the total number of voxels. To compute scaffold effective elasticity and permeability, we use a computational implementation of homogenization theory (20–22). The results for elasticity show that the effective stiffness matrix $[C^{\text{eff}}]$ is a function of the base scaffold stiffness matrix $[C]$, and a matrix that quantifies how the scaffold material is arranged in 3D space, $[M]$:

$$\underset{6\times6}{\left[C^{\text{eff}}\right]} = \frac{1}{|V|}\int_V \underset{6\times6}{[C]}\,\underset{6\times6}{[M]}\,\mathrm{d}V \tag{1}$$

where V is the volume of the unit cell. The results for permeability $[K^{\text{eff}}]$ show that it depends only on the average fluid velocity v of the porous structure:

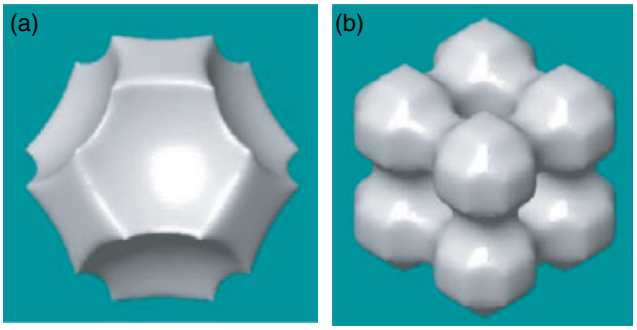

Fig. 1. Examples of designed architecture based on geometric equations: (a) interconnecting porous cylinders, and (b) interconnecting porous spheres.

$$\underset{3\times3}{\left[K^{\text{eff}}\right]} = \frac{1}{|V|}\int_V \underset{3\times3}{\begin{bmatrix} v_{01}^1 & v_{01}^2 & v_{01}^3 \\ v_{02}^1 & v_{02}^2 & v_{02}^3 \\ v_{03}^1 & v_{02}^2 & v_{03}^3 \end{bmatrix}} \mathrm{d}V \qquad (2)$$

Solving equations (1) and (2) gives us a quantitative measure of how a particular architecture will contribute to scaffold load bearing and biofactor delivery performance. We developed two interconnected porous architecture designs, one being an interconnected spherical pores and the other being interconnected cylindrical pores (Fig. 1).

Homogenization calculations of the effective moduli (Fig. 2a, normalized for the base moduli) and the permeability (Fig. 2b) demonstrate two important facts. First, with increasing volume fraction there is an increasing effective modulus, but decreasing permeability for both designs. This demonstrates the trade off faced in tissue engineering when trying to design scaffolds concurrently for load bearing (associated with modulus) and biofactor delivery (associated with permeability and interconnected porosity), namely that enhancing one design parameter comes at the detriment of the other design parameter. The second important fact is that the two different scaffold architectures demonstrate different stiffness for the same porosity as well as different permeability at the same porosity. This indicates within a given porosity changing architecture design will change both the load bearing and permeability characteristics of a scaffold.

The fact that modulus and permeability change inversely with porosity and that each are affected by scaffold architecture make it difficult to achieve target values for either through an *ad hoc* trial and error process. It is more efficient to utilize a mathematical algorithm that can sort through the various design combinations to find the right balance. This is the process of *optimization*. In optimization, we seek to minimize or maximize an objective function, which may be subject to constraints. In scaffold architecture design, we may seek to minimize the different between the scaffold modulus and a desired tissue target modulus, subject to the constraint that the scaffold must possess a desired level of porosity for biofactor seeding and delivery. An example scaffold optimization problem may be written formally as:

$$\text{Min}\left(\frac{C^{\text{scaffold}} - C^{\text{desired}}}{C^{\text{desired}}}\right)^2$$

Subject to: Scafford Porosity $\geq$ Desired Porosity

where C^{scaffold} is the designed scaffold stiffness and C^{desired} is the desired target stiffness. There are many ways to write a scaffold optimization problem, equation (3) being just one example.

We have developed two approaches to optimizing scaffold architecture, termed Restricted Architecture Topology Optimization (RATO, 1) and Full Architecture Topology Optimization (FATO, 23). In RATO, we characterize a class of architecture topology using a limited number of design parameters, hence the term

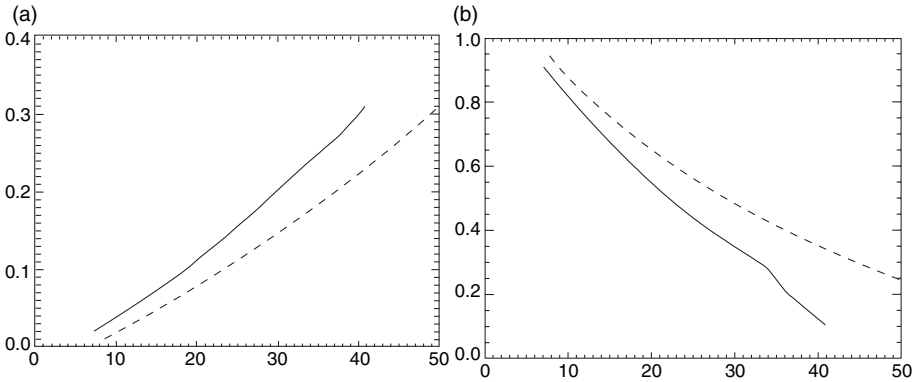

Fig. 2. Effect of designed architecture on scaffold elastic modulus and permeability. (a) Elastic modulus (normalized to the base material modulus) increases with increased volume fraction. The interconnecting sphere provides a stiffer scaffold than the interconnecting cylinders for any given porosity. (b) Permeability (normalized to a maximum permeability of 6) decreases with increasing volume fraction. The interconnecting cylinders provide greater permeability than the spheres for a given volume fraction.

'restricted'. For example, this class may be a set of interconnecting orthogonal cylinders that are characterized by the three cylindrical diameters. The effective moduli and permeability may then be computed using homogenization finite element analysis for the whole set of design diameters. A function is then fit between the effective moduli and pore diameter as well as effective permeability and pore diameter. This function may be fit using a polynomial and then run through a MATLAB^{TM} numerical optimization routine to find the pore diameters that allow the scaffold to best fit stiffness, porosity, and permeability requirements. Using this approach, we (25) have had success designing scaffolds to match target stiffness values for orthogonal moduli, but typically only when a high base biomaterial modulus (>2 GPa) is assumed. A second drawback is that it is difficult to match the complete directional or anisotropic bone stiffness of nine constants with only three design parameters.

Due to drawbacks in RATO, we developed a Full Architecture Topology Optimization (FATO) technique that would enable *de novo* scaffold architecture optimization without presumed topology (23). In this approach, a voxel database is used with each voxel having a potential volume fraction between 0 and 1. The material stiffness of an individual element is assumed to follow a power law with $C = C_{base}\rho^p$, where p is a coefficient >1. Based on the distribution of material density and local stiffness C, an effective stiffness tensor can be calculated using equation (1) after solving the elasticity homogenization equations. The homogenization solver is embedded into an optimization scheme with the Method of Moving Asymptotes (24) to update the density in each element. FATO provides a more flexible method of creating architecture with a capability of meeting a wider range of elastic constants. Figure 3 demonstrates a typical architecture created using FATO and the close match with native bone elastic properties of minipig mandibular condyle trabecular bone.

Once a designed architecture is created, and the global density image database is in place, we can perform simple Boolean operations to merge the image design databases. The density distribution from the global image design database is used to generate voxel locations into which the architecture image design voxel densities are substituted. The final result gives a designed scaffold that matches desired anatomic shape with microstructure designed to provide desired elastic, porosity and permeability characteristics. An example showing the entire design process for a Yucatan minipig mandibular condyle scaffold is shown in Fig. 4.

Scaffold fabrication

The scaffold designs created in the proceeding section are very complex 3D structures. In addition, increased design flexibility requires the capability to use materials with a wide range of material properties. Both of these requirements necessitate a sophisticated fabrication process that can make complex 3D structures from a range of biomaterials. Traditional machining or polymer processing techniques cannot make the complex structures created using image-based design techniques. Therefore, we use a set of technologies known as Solid Free-Form Fabrication (SFF). SFF techniques (see e.g. 25, 26) build structures using a layer by layer additive process and have been used to build a wide range of biomaterials. We use SFF techniques either to directly build the biomaterial scaffold, or to build a mold into which a biomaterial can be cast.

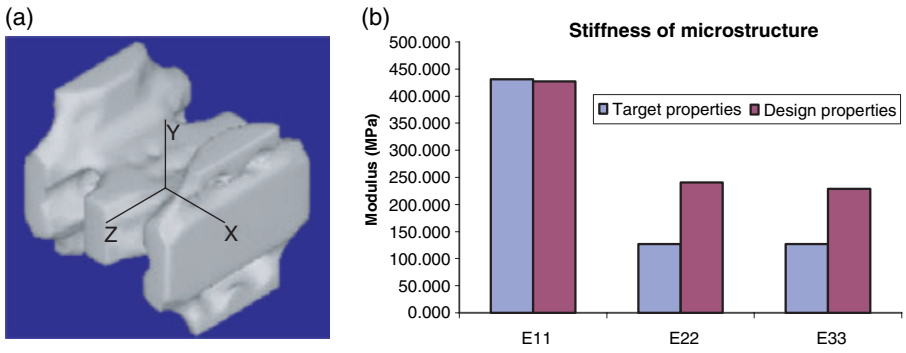

Fig. 3. (a) Example of an FATO architecture designed to match the anisotropic elastic moduli of minipig mandibular condyle trabecular bone. (b) Comparison of native condyle bone anisotropic moduli (blue) with designed scaffold anisotropic moduli (red).

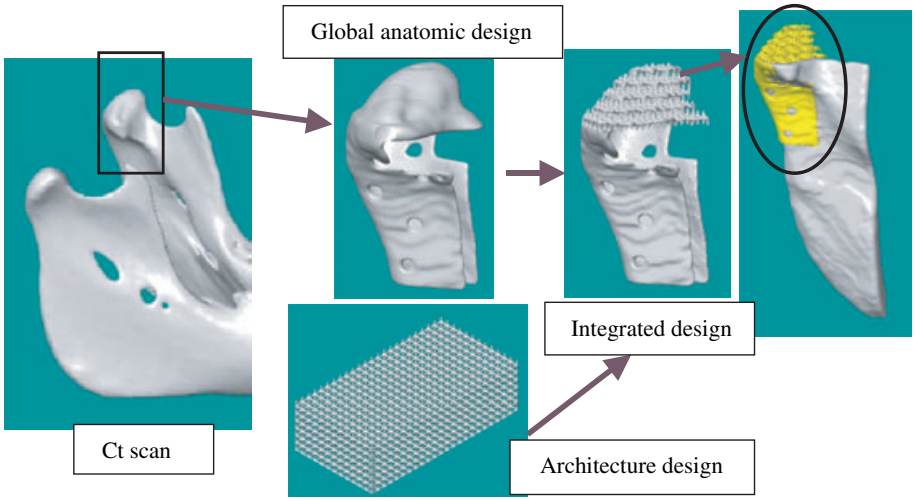

Fig. 4. Integrated image-based scaffold design process shown for a minipig mandibular condyle. The process begins with a CT or MR scan. A global image-design database is then created with surgical attachments. Next, a scaffold architecture is designed. Finally, the global anatomic and architecture data sets are combined to yield the final design which matches the original defect very well.

Although directly building the biomaterial scaffold on an SFF system is most desirable in terms of speed, it is often difficult as the biomaterial must be tailored to work with a particular machines building process. Our collaborative group has built two biomaterial scaffolds directly. First, we have built polycaprolactone (PCL) scaffolds directly on an SLS system (27). This technique uses powdered PCL within the SLS system and sinters the PCL particles together. Using this technique, we have been able to build complex anatomic scaffolds with designed architecture, including a Yucatan minipig mandibular condyle that matches closely the original condyle shape and includes a collar for surgical fixation (Fig. 5a). We have also, in collaboration with the Fraunhofer Institute for Laser Technology in Aachen Germany, have fabricated optimized scaffold architectures for spine fusion directly from titanium (Fig. 5b).

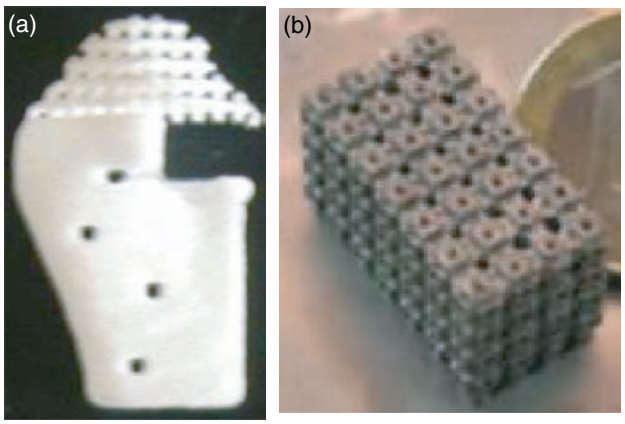

Fig. 5. Examples of scaffolds directly fabricated using SFF techniques. (a) The minipig mandibular condyle scaffold from Fig. 4 build directly from PCL. (b) A spinal fusion cage built directly from titanium.

A second approach to scaffold fabrication is indirect SFF. In this method, a mold is built from a design file and a biomaterial is cast into the mold (28, 29). The advantage of indirect SFF is that a wider range of biomaterials can be used for fabrication, including the construction of composite biomaterials. The disadvantage is significant increase in labor required to build the scaffolds. Using indirect SFF, we have fabricated scaffolds from hydroxyapatite (HA), tri-calcium phosphate (TCP), HA/TCP composites, polylactic acid (PLA), polyglycolic acid (PGA), polylactic/polyglycolic acid copolymers (PLGA), polypropylene fumarate/tri-calcium phosphate (PPF/TCP), and polycaprolactone (PCL). We have demonstrated the ability to build optimized designs, composite material and local/global porous scaffolds.

Structural and mechanical evaluation of designed scaffolds

There are two important questions concerning the actual fabricated scaffold load carrying capability relative to design characteristics. First, does the fabricated scaffold architecture actually match the design architecture? This is important because one failure of a fabricated scaffold to match designed performance could result from a mismatch between the actual architecture and the designed architecture. Second, do the actual fabricated scaffold mechanical properties

match the designed properties? If the designed architecture closely matches the fabricated architecture and the mechanical properties do not match, then the mismatch in scaffold properties could be attributed to a base material property in the actual scaffold that differs from the base property used in the scaffold design.

Our group has primarily utilized micro-computed tomography (μCT) scanning to evaluate fabricated scaffold architecture. For composite osteochondral scaffolds, we (29) have demonstrated using μCT that these scaffolds have truly interdigitated interfaces. To more rigorously examine how well the fabricated structure replicates the design structure, we can take a μCT scan of the actual fabricated structure and compare this directly to the scaffold design as the original scaffold design is also defined by image voxels. This comparison is done through image registration, where an algorithm matches one image data set to a second image data set using optimization algorithms. Using the image registration algorithm in ANALYZE^{TM} (http://www.analyzedirect.com/), we have been able to register an actual fabricated scaffold μCT voxel data set with a design voxel dataset. Subtracting the images shows that the designed titanium scaffold replicates the design well. Discrepancies can be seen do to particulate attachment on pore surfaces during the sintering process. Finally, the μCT scan/registration process can be used to assess structural changes during degradation, pinpointing precisely where material is lost. This can be readily done for *in vitro* degradation testing where the scaffold is placed in simulated body fluid at 37°C, and then periodically removed and μCT scanned. Results for PPF/TCP scaffold show areas of bulk degradation where the scaffold material density changes but not the geometry (Fig. 6).

In vitro mechanical evaluation should be done in concert with structural evaluation to best assess what determines scaffold mechanical performance initially and after degradation. *In vitro* mechanical testing is also important for evaluating computational models and improving scaffold design. A key component of scaffold mechanical testing is to utilize standard test specimens so that different scaffold designs and materials may be compared from different studies. There are a number of American Standards for Testing Materials (ASTM) and International Standard Organization (ISO) standards that govern mechanical specimen shape and procedures for both time 0 and degradation testing of biomaterials. In both cases, testing the *in vitro* behavior of scaffold architecture requires fabrication of the architecture within the test specimen geometry. We have done this for both compressive and tensile testing specimens (Fig. 7).

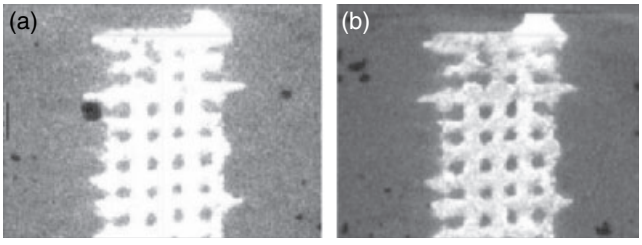

Fig. 6. Use of μCT scanning to assess scaffold degradation. (a) Scan of initial scaffold before degradation tests. (b) Scan after 12 weeks of *in vitro* degradation showing areas of radiolucency indicating degradation.

We have tested a range of biomaterials, both solid and porous, in compression, including HA, HA/TCP, PLGA, PPF/TCP, titanium, and PCL. Solid material testing is important for determining the upper bound of stiffness and strength, and to use as input for the optimization process. The mechanical properties of solid polymers depend on composition, molecular weight, and processing technique. The compressive properties of solid ceramics depend on composition as well as on sintering temperature. Represented compressive stiffness and modulus values for solid 50/50 PLGA, HA, PCL, and PPF/TCP are shown in Table 1.

Of course, solid biomaterials are not utilized for tissue engineering therapies but rather porous scaffolds. It is therefore critical to determine the mechanical properties of porous scaffold architectures. To date, we have performed compressive testing on scaffold architectures made from HA, PPF/TCP, PCL, 50/50 PLGA, and titanium with porosity ranging from 50 to 70% (Table 2).

The values for stiffness and strength for the polymer and polymer/ceramic composites range from 55 to 337 and 2 to 10 MPa, respectively, both of which are in the low to middle range for human trabecular bone structure reviewed in the Introduction. These results indicate that designed scaffolds will have sufficient load bearing properties for porosity below 60%. In addition, porous scaffold properties will also differ with different base stiffness, a reflection of different molecular weights for polymers, different sintering temperatures for ceramics, and the different processing techniques.

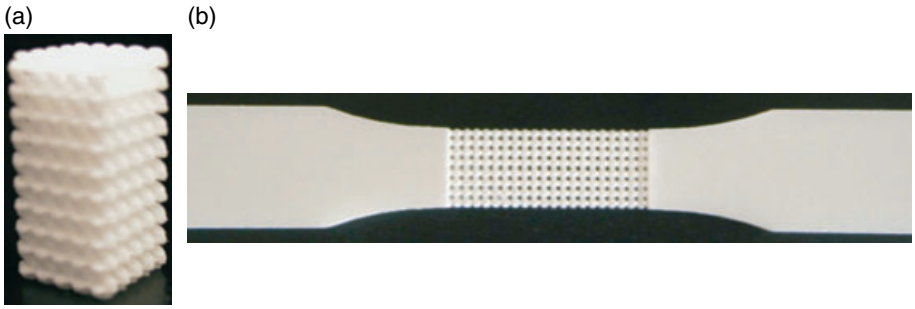

Fig. 7. Example of scaffold architecture mechanical test specimens fabricated to meet ASTM testing standards: (a) compressive test specimen, and (b) tensile test specimen.

Table 1. **Compressive modulus and strength of *solid* polymer and ceramic biomaterials used for craniofacial tissue engineering scaffolds**

Material	Compressive modulus (MPa)	Compressive strength (MPa)	Reference
50/50 PLGA	3103 ± 50	128 ± 1.7	30
PCL	122 ± 13	11.7 ± .5	27
PPF/TCP	543 ± 60	72.2 ± 14.3	Current paper
PPF	250 ± 40	41.9 ± 6.3	Current paper
TCP		14.0	31

PPF molecular weight: 3000 Da, weight percent: 23%.

Table 2. **Compression modulus and strength for designed porous polymer, ceramic and titanium biomaterial scaffolds used for craniofacial reconstruction. The strength notation for titanium of > 56 indicates that the material did not fail at 56 MPa which was the limit of the material testing system**

Scaffold material	Porosity (%)	Modulus (MPa)	Strength (MPa)	Reference
50/50 PLGA	50	337 ± 129	10.2	30
50/50 PLGA	70	90 ± 50	2.0	30
PCL	50	55 ± 3	2.3 ± 0.1	27
HA	39	1400 ± 400	30 ± 8	28
PPF/TCP	45	100	5	Current paper
Titanium	45	2700 ± 900	>56*	Current paper
TCP			3.5	31

In vivo **tissue regeneration on designed scaffolds**

The ultimate goal for scaffolds is to serve as a foundation for craniofacial skeletal tissue regeneration. Even if scaffold mechanical properties are adequate for temporary load bearing, failure to achieve enough tissue regeneration for functional support will ultimately still lead to mechanical failure. Therefore, it is important to determine *in vivo* tissue regeneration characteristics. Large animal models like minipigs are the ultimate test for functional tissue regeneration. However, due to expense and logistic difficulties of performing studies with the hundreds or thousands of large animals necessary to test the multitude of scaffold design variations, it is expedient to use small mouse and rat models. These models are easier to use in large numbers, but do not present the functional and volume challenges of large animal models that are needed to evaluate treatments for human application. Therefore, we have adopted a strategy of using a mouse model to screen a large number of scaffold design variables, and then testing the most promising scaffold design configurations in a large animal model.

There are a tremendous number of hybrid scaffold/biofactor variables that can affect tissue regeneration. These include the biofactor that is delivered, whether it is recombinant proteins, DNA plasmid, DNA delivered through viral vectors, progenitor or stem cells or combinations. In addition, the biofactor *carrier* (here we distinguish *carrier*, which only delivers the biofactor, vs. *scaffold*, which plays a mechanical role in addition to defining the 3D volume in which tissue grows), which includes hydrogels, polymer sponges, or ceramic particles can also affect biofactor activity and tissue regeneration. Finally, the scaffold itself may affect tissue regeneration either through cell–material interactions that can affect cell adherence and differentiation or through design in which the porous architecture can influence cell migration within that scaffold and nutrient/waste diffusion to/from cells within the scaffolds. Determining the best combination of biofactor/carrier/scaffold will depend upon performing relevant experiments in which all of these design variables can be rigorously controlled.

To date, we have studied how carriers, scaffold material and scaffold architecture affect bone regeneration. In terms of carriers, Schek et al. (32) found that

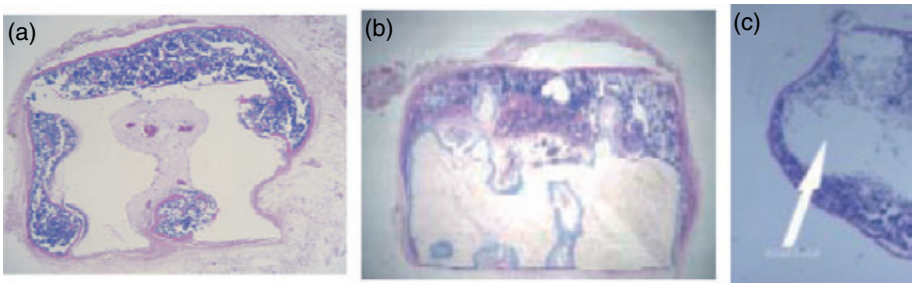

Fig. 8. Bone regenerate on three different scaffold materials using BMP-7 transduced human gingival fibroblasts in an immunocompromised mouse model: (a) HA, (b) PPF/TCP, and (c) PCL (white areas indicate where scaffold was removed for histological processing).

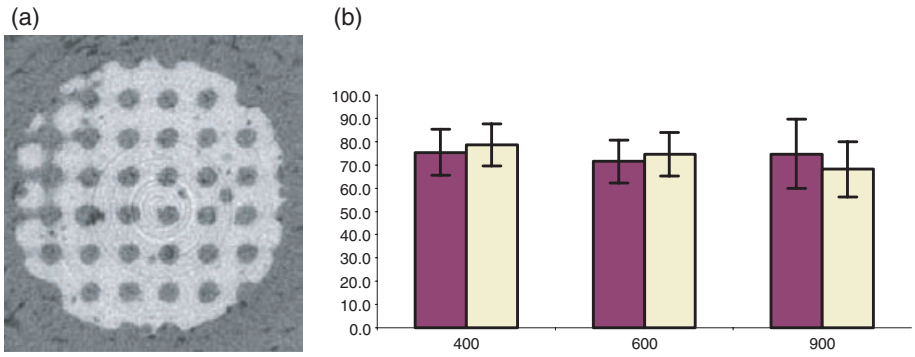

Fig. 9. Example of bone growth in designed HA scaffolds in a Yucatan minipig mandibular defect model. (a) Micro-CT scan slice showing bone (gray) penetrating through entire scaffold (white). (b) Bar graph showing total bone ingrowth between 70 and 80% at 18 weeks for pore sizes between 400 and 900 microns. No significant difference is seen between pore sizes.

fibrin gel loaded with viral vector carrying BMP-7 genes produced more bone in mouse quadriceps muscles then either collagen gel or virus in media. Subsequently using fibrin as a carrier, we have delivered human gingival fibroblasts transduced with BMP-7 from HA, PPF/TCP, and PCL scaffolds. All scaffold materials showed the capability to support bone formation in these models (Fig. 8). In a study on pore size, we found no statistical difference in the amount of bone formed in HA scaffolds with 300 or 800 μm pores. Taken together, these results suggest that the carrier is the most important factor in bone regeneration and scaffold material and especially pore size (for pores ranging from 300 to 800 μm) may play secondary roles.

We have also examined pore size and geometry issues using designed HA scaffolds in a Yucatan minipig mandibular defect model. In this study, we created three different pore designs, including a circular pore, square pore and circular strut, each with three different pore sizes for a total of nine designs. Pore diameters for the circular and square pores were 400, 600 and 900 μm and for the circular strut were 600, 900, and 1200 μm. Scaffolds were fabricated from HA using an indirect SFF approach and were 8 mm in diameter and 6 mm high. We implanted 20 empty scaffolds of each design for 6- and 18-week time points for a total of 720 scaffolds. Scaffolds were μCT scanned upon retrieval. Results indicated robust ingrowth at both 6 and 18 weeks, with bone occupying 40–50% of available pore volume at 6 weeks and 70–80% of available pore volume at 18 weeks (Fig. 9). No statistically significant difference was noted in total bone fill based on either pore size or pore geometry. Measuring bone penetration as bone fill in the innermost 1.5 mm of the scaffold, no significant difference was found between pore sizes or pore geometry at 18 weeks with innermost ingrowth ranging from 55 to 75%. At 6 weeks, pore sizes >600 μm had an innermost ingrowth of 10–16%. However, the 400 μm pore diameter design showed significantly less bone penetration, with innermost ingrowth of 4–8%. These results demonstrate that overall bone ingrowth did not depend on pore sizes between 400 and 1200 μm. Bone penetration may take longer in pore sizes of 400 μm. Although in contrast to other studies that have postulated an optimal pore size for bone ingrowth (references), it is important to note that these studies used scaffolds without controlled pore architecture. The reported pore diameter was a mean pore size, with a sizable distribution of pore sizes. Furthermore, the pore connectivity in these previous studies was not rigorously controlled.

Discussion and conclusions

In this paper, we have presented an approach for engineering craniofacial reconstruction scaffolds that is

a key part of a systematic approach for craniofacial tissue engineering. This approach integrates computational design, scaffold fabrication, scaffold structural and mechanical evaluation and *in vivo* tissue regeneration tests to develop scaffold/biofactor constructs that meet the anatomic shape, temporary load bearing and tissue regeneration requirements for craniofacial tissue engineering. Within this approach, we have demonstrated that image-based computational design techniques can be used to design scaffold architecture to meet both desired elastic properties for load bearing and permeability and pore interconnectivity requirements for tissue regeneration. We also demonstrated that these optimized architectures could be designed within any complex anatomic shape. Using SFF techniques, we have shown that complex designed scaffolds could be fabricated from a wide range of biomaterials including titanium, calcium-phosphate ceramics, and degradable polymer. These fabricated scaffolds exhibit mechanical stiffness/strength in the lower range of human trabecular bone, except for designed porous titanium which was in between cortical and trabecular bone. Scaffolds designed for degradation can retain mechanical stiffness/strength at significantly higher values than other designed scaffolds.

Designing and fabricating scaffolds with rigorously controlled architecture also allows more detailed experiments that test how both scaffold architecture and material affect tissue regeneration, as each can be varied independently. To date, we have extensively studied pore size (between 300 and 1200 μm) and material affects on bone regeneration. In both small and large animal models, there was significant bone regeneration in all pore sizes ranging from 300 to 1200 μm, with no pore size being statistically different. Also, bone regeneration was found to occur in a number of materials, including HA, PPF/TCP, and PCL. These results suggest that pore size and material may not play as significant of a role in tissue regeneration as carrier and biofactor.

Craniofacial reconstruction by tissue engineering requires complex synergy of a multitude of biofactor, carrier and scaffold factors to provide constant function through to functional tissue. The ability to control as many variables as possible is necessary to determine the optimal treatment regimen. Although we have demonstrated the capability to control scaffold material and architecture variables, these must be rigorously tested in functional models to determine what scaffold materials and architecture are best for tissue regeneration. For example, although scaffolds can be engineered to match some percentage of native tissue stiffness/strength, biomaterial limitations make it difficult to exactly match native tissue values. The question then becomes whether mechanical properties attainable through material synthesis and design are adequate for functional *in vivo* loading. This can only be tested in large functional animal models.

A second but equally critical question is how the scaffold will affect tissue regeneration through biofactor delivery. We have found that pore sizes in the range of 300–1200 mm do not have a significant influence on bone regeneration in that we see robust bone formation for all these pore sizes. Other factors, including porosity and permeability (a measure of pore connectivity) must be tested to determine if there is an optimal value for these parameters. This again will require the use of scaffolds with rigorously controlled architecture tested in both small and large animal models. We do now have the integrated engineering platform in place to test all of these questions concerning load bearing and tissue regeneration. Furthermore, these engineering techniques can create scaffolds that are suitable for use in clinical applications. The continued concurrent engineering and testing of scaffold/biofactor hybrids will optimize the approach for human patients.

Acknowledgements: The authors gratefully acknowledge support for studies reported in this paper from the NIH NIDCR through DE 13608 (Bioengineering Research Partnership) and DE 13416. We would also like to thank Professors Antonio Mikos and Michael Yaszemski for providing the PPF material.

References

1. Hollister SJ, Maddox RD, Taboas JM. Optimal design and fabrication of scaffolds to mimic tissue properties and satisfy biological constraints. *Biomaterials* 2002;**23**:4095–103.
2. Hutmacher DW. Scaffolds in tissue engineering bone and cartilage. *Biomaterials* 2000;**21**:2529–43.
3. Yaszemski MJ, Payne RG, Hayes WC, Langer R, Mikos A. Evolution of bone transplantation: molecular, cellular and tissue strategies to engineer human bone. *Biomaterials* 1995;**17**:175–85.
4. Schwartz-Dabney CL, Dechow PC. Accuracy of elastic property measurement in mandibular cortical bone is improved by using cylindrical specimens. *J Biomech Eng* 2002;**124**:714–23.
5. Schwartz-Dabney CL, Dechow PC. Edentulation alters material properties of cortical bone in the human mandible. *J Dent Res* 2002;**81**:613–7.

6. Schwartz-Dabney CL, Dechow PC. Variations in cortical material properties throughout the human dentate mandible. *Am J Phys Anthropol* 2003;**120**:252–77.
7. Giesen EB, Ding M, Dalstra M, van Eijden TM. Changed morphology and mechanical properties of cancellous bone in the mandibular condyles of edentate people. *J Dent Res* 2004;**83**:255–9.
8. Giesen EB, Ding M, Dalstra M, van Eijden TM. Mechanical properties of cancellous bone in the human mandibular condyle are anisotropic. *J Biomech* 2001;**34**:799–803.
9. O'Mahony AM, Williams JL, Katz JO, Spencer P. Anisotropic elastic properties of cancellous bone from a human edentulous mandible. *Clin Oral Implants Res* 2000;**11**:415–21.
10. Dechow PC, Hylander WL. Elastic properties and masticatory bone stress in the macaque mandible. *Am J Phys Anthropol* 2000;**112**:553–74.
11. Ashman RB, Rosinia G, Cowin SC, Fontenot MG, Rice JC. The bone tissue of the canine mandible is elastically isotropic. *J Biomech* 1985;**18**:717–21.
12. Detamore MS, Athanasiou KA. Motivation, characterization, and strategy for tissue engineering the temporomandibular joint disc. *Tissue Eng* 2003;**9**:1065–87.
13. Hu K, Radhakrishnan P, Patel RV, Mao JJ. Regional structural and viscoelastic properties of fibrocartilage upon dynamic nanoindentation of the articular condyle. *J Struct Biol* 2001;**136**:46–52.
14. Patel RV, Mao JJ. Microstructural and elastic properties of the extracellular matrices of the superficial zone of neonatal articular cartilage by atomic force microscopy. *Front Biosci* 2003;**8**:a18–25.
15. Fong KD, Nacamuli RP, Song HM, Warren SM, Lorenz HP, Longaker MT. New strategies for craniofacial repair and replacement: a brief review. *J Craniofac Surg* 2003;**14**:333–9.
16. Hollinger JO, Winn SR. Tissue engineering of bone in the craniofacial complex. *Ann N Y Acad Sci* 1999;**875**:379–85.
17. Warren SM, Fong KD, Chen CM et al. Tools and techniques for craniofacial tissue engineering. *Tissue Eng* 2003;**9**:187–200.
18. Isogai N, Landis W, Kim TH, Gerstenfeld LC, Upton J, Vacanti JP. Formation of phalanges and small joints by tissue-engineering. *J Bone Joint Surg Am* 1999;**81**:306–16.
19. Hollister SJ, Levy RA, Chu TM, Halloran JW, Feinberg SE. An image-based approach for designing and manufacturing craniofacial scaffolds. *Int J Oral Maxillofac Surg* 2000;**29**:67–71.
20. Hollister SJ, Brennan JM, Kikuchi N. A homogenization sampling procedure for calculating trabecular bone effective stiffness and tissue level stress. *J Biomech* 1994;**27**:433–44.
21. Sanchez-Palencia E, Zaoui A. In: Araki H, Kyoto J et al., editors. *Homogenization Techniques for Composite Media, Lecture Notes in Physics*. New York: Springer-Verlag; 1987. 272 pp.
22. Hornung U (ed). *Homogenization and Porous Media*. Interdisciplinary Applied Mathematics. New York: Springer-Verlag; 1997.
23. Lin CY, Kikuchi N, Hollister SJ. A novel method for biomaterial scaffold internal architecture design to match bone elastic properties with desired porosity. *J Biomech* 2004;**37**:623–36.
24. Svanberg K. The method of moving asymptotes – a new method for structural optimization. *Int J Num Meth Eng* 1987;**24**:359.
25. Hollister SJ, Taboas JM, Schek RM, Lin CY, Chu TM. Design and fabrication of bone tissue engineering scaffolds. In: Hollinger JO, editor. *Bone Tissue Engineering*. CRC Press, 2005.
26. Hutmacher DW, Sittinger M, Risbud MV. Scaffold-based tissue engineering: rationale for computer-aided design and solid free-form fabrication systems. *Trends Biotechnol* 2004;**22**:354–62.
27. Das S, Adewunmi B, Williams JM, Flanagan CL, Engel A, Hollister SJ et al. Mechanical and structural properties of polycaprolactone scaffolds made by selective laser sintering. *Proceedings of the 7th World Biomaterials Congress*, Sydney, 2004.
28. Chu TM, Orton DG, Hollister SJ, Feinberg SE, Halloran JW. Mechanical and in vivo performance of hydroxyapatite implants with controlled architectures. *Biomaterials* 2002;**23**:1283–93.
29. Taboas JM, Maddox RD, Krebsbach PH, Hollister SJ. Indirect solid free form fabrication of local and global porous, biomimetic and composite 3D polymer-ceramic scaffolds. *Biomaterials* 2003;**24**:181–94.
30. Diggs A, Hollister SJ, Chu TM. Fabrication and characterization of 3D biphasic ceramic scaffolds composed of hydroxyapatite and b-tricalcium phosphate. *Proc Soc Biomater* 2003;353.
31. Saito E, Flanagan CL, Taboas JM, Hollister SJ. Computational and experimental mechanical properties of designed 50/50 PLGA scaffolds made by indirect solid free-form fabrication. *Trans Orthop Res Soc* 2004;**29**:745.
32. Schek RM, Hollister SJ, Krebsbach PH. Delivery and protection of adenoviruses using biocompatible hydrogels for localized gene therapy. *Mol Ther* 2004;**9**:130–8.